Anomalous elastic behavior of relaxor ferroelectric $Ca_{0.28}Ba_{0.72}Nb_2O_6$ single crystals

Chandra Shekhar Pandey* and Jürgen Schreuer†
Institute for Geology, Mineralogy and Geophysics, Ruhr-University Bochum, Universitaetsstrasse 150, D-44801 Bochum, Germany

Manfred Burianek and Manfred Mühlberg
Institute for Crystallography, University of Cologne, Zülpicher Strasse 49b, 50674 Cologne, Germany
(Received 5 July 2011; revised manuscript received 21 September 2011; published 7 November 2011)

Full sets of elastic constants c_{ij} of tetragonal tungsten bronze relaxor ferroelectric $Ca_{0.28}Ba_{0.72}Nb_2O_6$ (CBN-28) single crystals are measured above Curie temperature up to 1503 K employing resonant ultrasound spectroscopy. Thermal expansion measurements on as-grown unpoled CBN-28 reveal the existence of a characteristic temperature T^* (∼800 K) for CBN-28 between the Burns temperature T_b (∼1100 K) and the temperature of maximum dielectric permittivity T_m (∼600 K). The influence of polar nanoregions (PNRs) on the elastic properties of CBN-28 is studied in detail. The temperature evolution of c_{ij} shows pronounced anomalies. All independent elastic constants evolved differently, with temperature reflecting their coupling to different types of the reorientational motion of PNRs through their interaction with acoustic waves. The anisotropy of longitudinal elastic stiffness coefficients and the deviation from Cauchy relations for CBN-28 are also studied, showing the evolution of material anisotropy and the nature of bonding interactions with temperature, respectively.

DOI: 10.1103/PhysRevB.84.174102 PACS number(s): 77.80.−e, 62.20.de, 62.65.+k, 65.40.De

I. INTRODUCTION

Relaxor ferroelectric materials (or relaxors) have been of great interest for last half-century because of their unique physical properties[1,2] and a wide range of technological applications.[3,4] Rigorous research on relaxors reveals the following characteristics: (1) the occurrence of a diffuse phase transition over a temperature range near the temperature T_m, at which the measured real part of the dielectric constant passes through a maximum instead of an abrupt ferroic transition at the Curie temperature T_c, and (2) the appearance of the Burns temperature T_b[5] (several hundred degrees above T_m),[6] where nucleation of dynamic polar nanoregions (PNRs) begins. The latter system is called the ergodic (violated paraelectric) state, consisting of randomly oriented dynamic PNRs. Upon cooling, the average size of PNRs increases; however, their dynamics slow down.[7] With further cooling below T_m, the PNRs either freeze at T_f, leading to a nonergodic stage (glassylike) for canonical relaxors, or a diffuse "relaxor-to-ferroelectric" phase transition takes place at T_c.[8] Neutron scattering experiments on $PbZn_{1/3}Nb_{2/3}O_3$ reveals the existence of an intermediate temperature T^*[9,10] between T_b and T_f where initial freezing of the PNRs begins. Extended studies on T^*[11–18] revealed that T^* is a common feature of lead-based relaxors. Finally, we can conclude that four major characteristic temperatures occur in relaxors: (1) T_b, the temperature for the initiation of dynamic PNRs; (2) T^*, the temperature at which the freezing of PNRs begins; (3) T_m, the temperature at which the dielectric maxima occurs and a quasistatic behavior of PNRs exists; and (4) T_f (below T_m), the temperature below which the PNRs are static. The PNRs strongly affect the relaxor properties, and their existence has been proved experimentally[8]; however, the phenomena behind their formation are still unknown. Their presence can be noticed in various ways, e.g., changes in the sound velocity and the corresponding elastic constant at T_b,[19] measurements of thermal properties (thermal expansion coefficients and strain),[2,5,20–22] anomalies in the specific heat,[23] deviation from the Curie-Weiss law,[24] and dynamic slowing down through the Vögel-Fulcher relationship.[25]

For a few decades, much focus was on lead-based relaxors like $PbMg_{1/3}Nb_{2/3}O_3$[26] and related compounds.[27–29] However, the volatility and toxicity of PbO is the main disadvantage of lead-based relaxors. Therefore, more research is encouraged in the field of lead-free relaxors. Among various reported lead-free relaxors, $Sr_xBa_{1-x}Nb_2O_6$ (SBN-x) with $x \approx 0.61$ (SBN-61, hereafter SBN) has attracted much interest because of its outstanding pyroelectric,[30] piezoelectric,[31] electro-optic,[32,33] and photorefractive properties[34–37] and its surface acoustic wave device applications.[38] SBN crystallizes in the partially filled tetragonal tungsten bronze (TTB) structure type. The ferroelectric phase transition temperature of the congruent melting SBN is ∼352 K,[39] which implies that SBN crystals may be easily depolarized near room temperature. Therefore, it has become necessary to search for new materials that are closely related to SBN structurally but have a much higher Curie temperature. Another member of the partially filled TTB structure family is $Ca_xBa_{1-x}Nb_2O_6$ (CBN-x, with $0.20 \leqslant x \leqslant 0.40$[40]), which was first reported by Ref. 41. The first single crystals of $Ca_{0.28}Ba_{0.72}Nb_2O_6$ (CBN-28, hereafter CBN) were grown by the authors of Ref. 42; CBN is a potential alternative to SBN for device applications because of its relatively high Curie temperatures at 537 K, ∼200 K higher than those of SBN. The high-temperature paraelectric phase of CBN is tetragonal, with the point symmetry $4/mmm$, and the low-temperature ferroelectric phase is also tetragonal but with a point symmetry of $4mm$.

Various authors have focused on different aspects of CBN, including studies of dielectric, ferroelectric, and optical properties[42–46]; ferroelectric domain structure and its evolution using transmission electron microscopy[39]; phase diagram analysis[47]; and room temperature–specific heat, together with thermal expansion coefficients in the temperature range 298–573 K.[46] However, the elastic constants of CBN single crystals are unknown to date. Moreover, the detailed relaxor phenomena, together with the existence of T_b, T^*, and T_m, has

not yet been reported for TTB relaxor CBN. Hence, the aim of this work is to gain more insight into the relaxor phenomena in CBN by studying its thermal expansion behavior and the temperature dependence of full sets of elastic constants above T_c. To this end, we employ a combination of experimental techniques, including differential scanning calorimetry, high-resolution dilatometry, and the innovative method of resonant ultrasound spectroscopy (RUS). In RUS, the elastic constants are derived from the resonance frequencies of a freely vibrating sample,[48] which allows determination of all independent elastic constants on a single sample in one measurement with high internal consistency.[49]

II. EXPERIMENTAL DETAILS

A. Sample preparation

All physical properties reported here are referred to a Cartesian reference system. Its basis vectors $\vec{e}_i$ are related to the basis vectors $\vec{a}_i$ of the crystallographic reference system according to $\vec{e}_i \parallel \vec{a}_i$. One large light yellow to transparent single crystal of CBN was grown by the Czochralski method.[40] Two rectangular parallelepipeds (named CBN-0201 and CBN-0202), with edges parallel to $\vec{e}_i$ and an edge length in the range 6–8 mm, were cut from the large single crystal and polished to optical quality. The orientation of the samples was controlled by Laue backscattering and Bragg diffraction techniques. Deviations from ideal orientation were less than 0.3°. Opposite faces were parallel to within ± 1 μm. The calculated geometric density $\rho_g = M/l_1 l_2 l_3$ (M is the sample mass and l_i are the edge lengths) matches well the density obtained by the buoyancy method, confirming the high quality of the samples, particularly in respect to geometrical errors. Final sample dimensions are given in Table I.

B. Phase transition

The phase transition temperature of CBN was observed with the aid of a differential scanning calorimeter (DSC 404 F1 Pegasus)[50] in a He purge gas atmosphere.

TABLE I. Characterization of CBN samples.[a]

Sample name	CBN-0201[b]	CBN-0202[b]
Structure type	Partially filled TTB	
Space group	$P4bm$ (at room temperature)	
Melting point	>1460 °C	
Ferroelectric transition	$T_c = 264.4$ °C ($4mm \leftrightarrow 4/mmm$)	
Optical quality	Light yellow to transparent inclusion free single crystal	
a (Å)	12.4491(5)	
c (Å)	3.95858(7)	
V (Å)	613.30(4)	
l_1 (mm)	7.493(2)	7.370(1)
l_2 (mm)	6.407(1)	7.972(1)
l_3 (mm) $\parallel$ c-axis	7.436(1)	7.519(1)
ρ_b (gm/cc)	5.302(2)	
ρ_g (gm/cc)	5.292(5)	5.299(3)

[a]Lattice parameters are taken from Ref. 40.
[b]Uncertainty of the last decimal is in parenthesis.

C. Thermal expansion

The thermal expansion coefficient, a second rank tensor, is a typical anharmonic property of the crystal lattice. The determination of accurate temperature coefficients of elastic constants requires the correction of changes in sample dimensions and density because of thermal expansion. Therefore, thermal expansion measurements (temperature range 100–1523 K) were performed on CBN rectangular parallelepipeds using a commercial inductive gauge dilatometer (DIL 402 C).[50] The measurements were performed in two overlapping temperature ranges, 100–673 K in a He purge gas atmosphere and 296–1523 K in air using a low-temperature and a high-temperature furnace, respectively. Expansion of the samples was measured while applying heating/cooling rates of 1 K/min. Each run was repeated at least two times to test the reproducibility of the observed strains. Data from the corresponding low- and high-temperature runs were merged for further data analysis.

D. Elastic constants

Resonance spectra on both samples were collected up to 1503 K using a high-temperature RUS device built in house. The device consists of a commercial furnace (type 6.219.1-20)[50] equipped with two thermocouples of type S, one located close to the sample and the other close to the SiC heating element of the furnace. Temperature control was achieved by a cascading controller (EPC900 from Eurotherm) in connection with a 2-kVA direct current power supply (HP6674A from Agilent). At the position of the sample, the temperature was stable within ± 0.1 K and the accuracy was better than ± 5 K at 1503 K. The resonance spectra were collected using a network analyzer (HP 4194A from Agilent). The electric signals were amplified up to 20 times (in case of a weak signal from the sample) using a high-speed power amplifier (BA4825).[51] The rectangular parallelepipeds were weakly clamped at opposite corners between two rods made of corundum ceramics, which act simultaneously as ultrasonic transducer rods and as the sample holder. To approach the boundary conditions of a freely vibrating body, the mechanical load on the sample was kept below 0.03 N.

At least 120 eigenfrequencies in the range 200–1140 kHz were extracted from each resonance spectrum and used in nonlinear least-square refinements, minimizing the quantity $\chi^2 = \sum_{i=1}^{n} w_i((\omega_i^2)_{\mathrm{calc}} - (\omega_i^2)_{\mathrm{obs}})^2$ for n circular eigenfrequencies ($\omega_i = 2\pi\nu_i$) by adjusting the values of the elastic constants c_{ij}. $(\omega_i)_{\mathrm{calc}}$ is the ith calculated frequency, and $(\omega_i)_{\mathrm{obs}}$ is the ith observed one. The w_i are individual weights calculated by assuming an experimental error of ± 0.1 kHz for each observed resonance frequency. After correcting the sample dimensions and density due to thermal expansion effects (directly derived from the calibration-corrected dilatometric strains measured on the same sample), the elastic constants at each temperature were successively refined using the final c_{ij} obtained at the previous temperature step as the starting model. The initial model at 1083 K was derived from the elastic constants of SBN,[52] taking into account well-known rules for the elastic behavior of chemically and structurally related compounds.[53,54] At least four resonance spectra (heating–cooling–heating–cooling) were collected on each sample at elevated temperatures to check the reproducibility

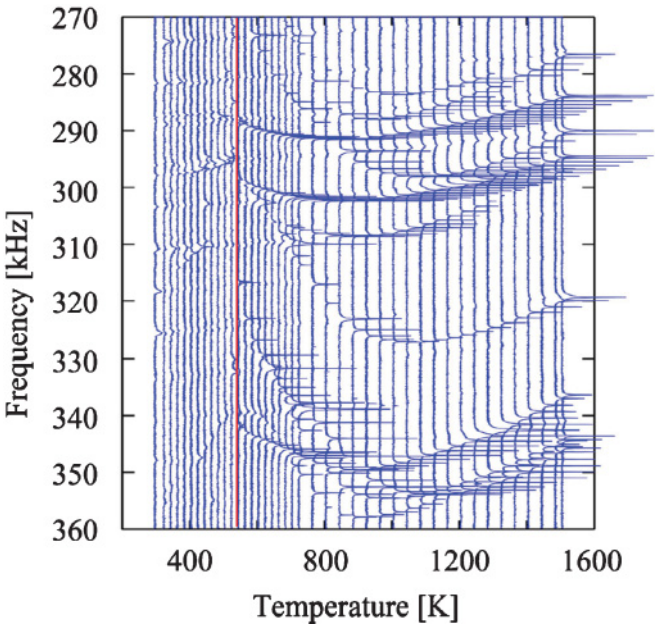

FIG. 1. (Color online) Part of the resonance spectra of CBN. The ferroelectric phase transition temperature is shown by a red line.

of elastic constants. Fully reproducible resonance spectra were observed. Part of the resonance spectra is shown in Fig. 1. The ferroelectric phase transition temperature ($T_c \sim 537$ K) is shown by a red line. In the following section, we discuss our results on thermal expansion and elastic properties of as-grown unpoled CBN single crystals.

III. RESULTS AND DISCUSSION

A. Phase transition

The ferroelectric phase transition ($4mm \leftrightarrow 4/mmm$) was observed at 537.4 K (T_c) (lower curve in Fig. 2), and the transition temperature of the light yellow to transparent CBN crystals is well reproducible. However, heating CBN in a He atmosphere at temperatures above ~650 K started to change its color from transparent to bluish, with T_c shifted to higher temperatures by ~5.4 K (upper curve in Fig. 2), which turns into dark blue on heating to 1503 K. Both the shift in T_c and the color change are found to be reversible after annealing the blue crystal in air at 1273 K for 3 h. These effects are probably caused by oxygen deficiency at high temperatures, leading to a reduction[55] of $Nb^{5+} \rightarrow Nb^{4+}$, and vice versa when the crystal is annealed in air, as reported for SBN on its color change.[56,57]

B. Thermal expansion

The ferroelectric and paraelectric phases of CBN are tetragonal and hence have only two independent principal thermal expansion coefficients[58]: α_{11} ($=\alpha_{22}$) and α_{33}. Calibration-corrected strains, together with linear thermal expansion coefficients along the crystallographic a-($=b$-) and c-axes, are shown in Fig. 3, and linear thermal expansion coefficients (first derivative of the corresponding strain curves) at selected temperatures are tabulated in Table II. The temperature-induced strains show a nonlinear and anisotropic behavior in the measured temperature range. Along the c-axis, the strain

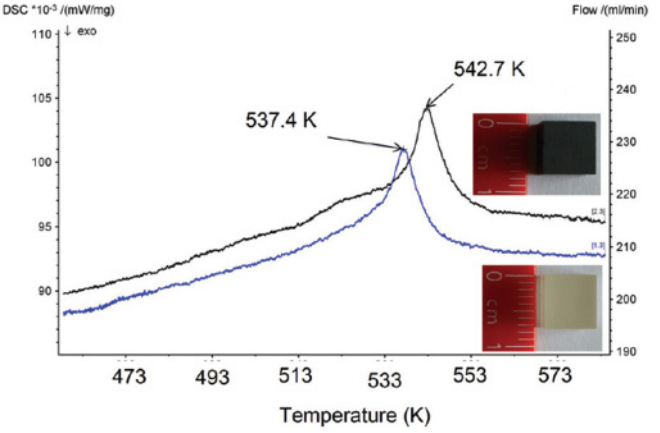

FIG. 2. (Color online) Shifting of the ferroelectric transition temperature of CBN before (blue curve, transparent crystal) and after (black curve, dark blue crystal) heating in a He purge gas atmosphere.

remains positive from 100 K to ~300 K, followed by a negative thermal expansion in the temperature regime of $300 \leqslant T \leqslant T_c$ and positive expansion thereafter. In thermal expansion curves along the a- [Fig. 3 (a)] and c- [Fig. 3 (b)] axes, there exist three distinct points of deviation from linearity above T_c: ~600 K, ~800 K, and ~1100 K. The negative thermal expansion

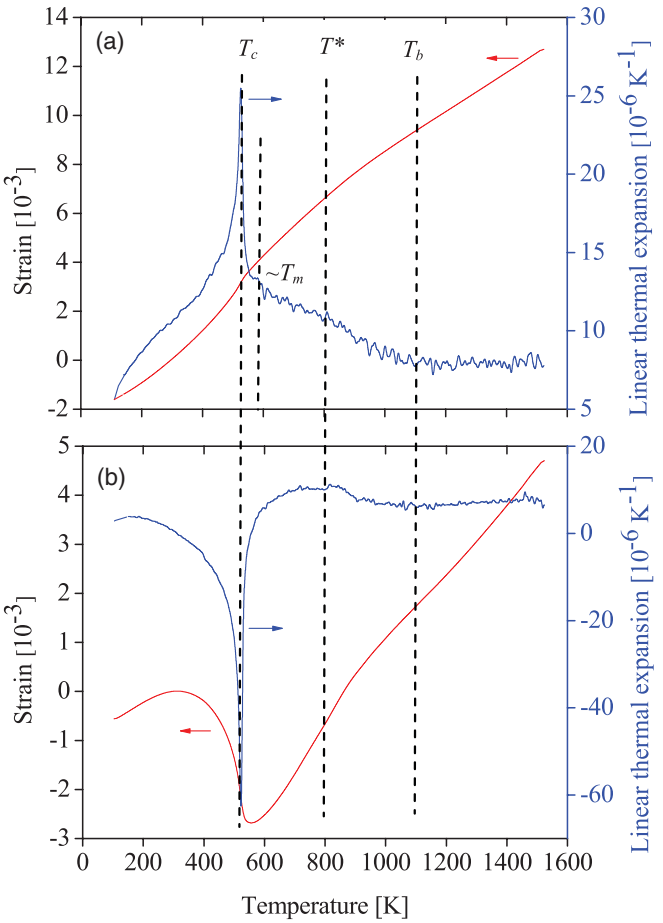

FIG. 3. (Color online) Temperature-induced strains and corresponding linear thermal expansion (a) perpendicular and (b) parallel to the c-axis.

TABLE II. Elastic properties of CBN at selected temperatures.

T (K)	563	723	843	1003	1243	1503
c_{11}[a]	217.6(2)	221.6(2)	229.1(2)	230.2(1)	223.9(1)	213.8(1)
c_{33}[a]	143.5(3)	158.1(2)	170.8(2)	183.3(2)	186.2(2)	181.0(2)
c_{44}[a]	69.9(1)	69.8(1)	69.4(1)	68.6(1)	67.2(1)	65.3(1)
c_{66}[a]	75.4(2)	76.6(1)	76.8(1)	76.2(1)	73.6(1)	70.6(1)
c_{12}[a]	99.9(4)	90.8(2)	85.0(2)	85.5(2)	84.1(2)	81.4(2)
c_{13}[a]	60.2(3)	57.0(2)	61.4(2)	67.2(2)	69.1(2)	68.6(2)
g_{11}[a]	−9.7	−12.8	−7.9	−1.4	+1.9	+3.3
g_{33}[a]	+24.5	+14.3	+8.2	+9.4	+10.3	+10.8
B[a]	105.3	107.0	112.5	118.1	118.3	115.0
$c'_{\max}/c'_{\min}$[b]	1.63	1.47	1.37	1.28	1.22	1.21
T_{11}[c]	0.0(2)	2.3(2)	1.85(6)	−0.60(1)	−1.50(1)	−2.08(1)
T_{33}[c]	10(2)	4.5(1)	7.3(2)	2.24(4)	−0.51(7)	−1.55(9)
T_{44}[c]	−0.3(3)	−0.26(1)	−0.61(1)	−0.77(1)	−0.98(1)	−1.21(1)
T_{66}[c]	2.1(6)	0.52(1)	−0.07(4)	−0.91(1)	−1.52(1)	−1.97(2)
T_{12}[c]	−4.1(5)	−7.5(9)	−1.3(3)	−0.16(7)	−0.96(2)	−1.51(6)
T_{13}[c]	6.0(9)	1.4(6)	9.7(2)	2.8(1)	0.10(6)	−0.51(9)
α_{11}[d]	13.4(2)	11.5(1)	10.5(1)	8.6(1)	8.5(1)	8.7(1)
α_{33}[d]	1.4(2)	10.2(1)	11.1(1)	7.0(1)	7.2(1)	8.0(1)
α_V[d]	28.2	33.2	32.1	24.2	24.2	25.4

[a]Elastic constants c_{ij}, deviations from Cauchy relations g_{ij}, and bulk modulus B are in gigapascals.
[b]The ratio of maximal and minimal longitudinal elastic stiffness $c'_{\max}/c'_{\min}$ is dimensionless.
[c]Thermoelastic constants $T_{ij} = \mathrm{d}\log c_{ij}/\mathrm{dT}$ are in 10^{-4} reciprocal kelvins.
[d]Coefficients of linear thermal expansion α_{ij} and of volume thermal expansion $\alpha_V = 2\alpha_{11} + \alpha_{33}$ are in 10^{-6} reciprocal kelvins.

along the c-axis above room temperature suggests that the structural changes start at ∼300 K and end at ∼550 K. These results are comparable to those observed for SBN crystals by various authors,[59–61] who reported that the structural changes corresponding to the onset of the ferroelectric phase transition are responsible for the anomalies in thermal expansion.

Let us focus on distinct deviations from linearity observed above T_c in the temperature evolution of strain along and perpendicular to the c-axis (Fig. 3). These three distinct deviations from linearity can be seen more clearly in the temperature evolution of the coefficients of thermal expansion of ∼600 K, ∼800 K, and ∼1100 K. The first deviation from linearity at temperature of ∼1100 K corresponds to Burns temperature T_b, where the initiation of PNRs occurs, and has been suggested as a common feature of relaxor ferroelectrics.[5] The second nonlinearity ∼800 K corresponds to T^*, where the initial freezing of dynamic PNRs begins, and extends to T_m. The third deviation ∼600 K may be considered T_m. However, detailed dielectric measurements are needed to confirm the exact number for T_m. All characteristic temperatures T_c, T_m, T^*, and T_b for CBN are shown in Fig. 3. The position of T_f was not identified in our measurements of thermal expansion, which suggests the occurrence of a diffuse "relaxor-to-ferroelectric" phase transition in CBN, based on the existence of T_f being undetectable in such a transition because the ergodic stage at T_c is found nearly close to T_f.[8]

C. Elastic properties

The paraelectric phase of CBN has a tetragonal structure with the point symmetry $4/mmm$, which has six symmetry-independent elastic constants (c_{11}, c_{33}, c_{12}, c_{13}, c_{33}, c_{44}, and c_{66}).[58] According to the Voigt notation, the longitudinal elastic stiffness coefficients c_{11} and c_{33} are related to the longitudinal acoustic (LA) waves whose wavevectors are in plane perpendicular and parallel to the polar c-axis, respectively. The shear stiffness coefficients c_{44} and c_{66} are related to transverse acoustic (TA) waves propagating in the [001] and [100] directions, respectively, and polarized in the [010] direction. The transverse interaction coefficients c_{12} and c_{13} do not control any acoustic waves but are related to the combination of different LA and TA waves. The elastic constants calculated from the observed resonance spectra are shown in Fig. 4 in a relative scale, and individual values at selected temperatures are presented in Table II. The full sets of elastic constants measured on both investigated samples are in excellent agreement, indicating the high precision of our RUS setup, as well as the gem quality of the samples. The elastic constants c_{ij} of the individual samples deviate only by 0.4% from the corresponding averaged values at high temperatures. However, this deviation is slightly larger (1.0%) near T_c because of strong ultrasound attenuation.

Temperature evolution of c_{ij} above T_c shows strong and pronounced anomalies, as depicted in Fig. 4. On cooling from high temperature, all elastic constants behave differently with temperature. The constant c_{11} shows a small softening on cooling below T_b, while c_{33} experiences much faster softening. This softening is related to the growth of dynamic PNRs accompanied by the local strains and their interaction with phonons.[62] On further cooling, both coefficients deviate from their behavior and the softening is reduced significantly at ∼800 K (T^*). This "reduced softening" can be attributed to the appearance of static PNRs. On further cooling below T^*, all PNRs are correlated, which probably leads to saturation of

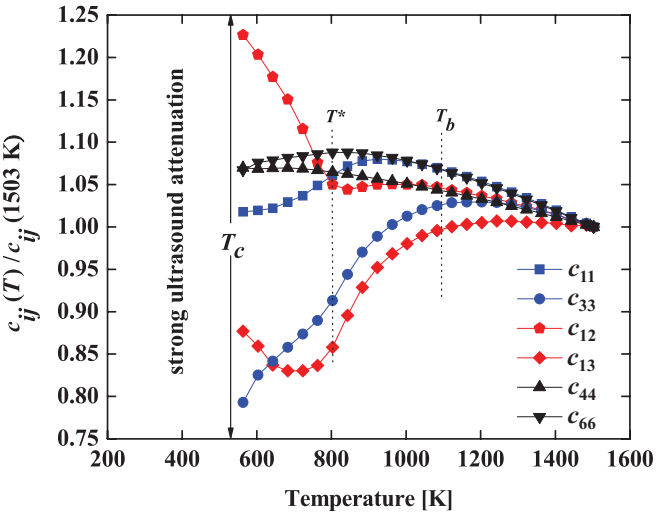

FIG. 4. (Color online) Temperature dependence of relative elastic constants $c_{ij}(T)/c_{ij}$(1503 K) above T_c.

c_{11} on approaching T_m. However, c_{33} still displays significant softening near T_m, indicating that the small dynamic PNRs are still present and couple with the corresponding LA waves.

The shear stiffness coefficients c_{44} and c_{66} show very weak or no substantial anomalies. This can be correlated with the growing sizes of the PNRs on cooling, whose reorientational motions are suppressed by the shear strain of the TA waves in related directions. The transverse interaction coefficients c_{12} and c_{13} display quite different behavior on cooling, compared to the rest of the elastic constants. On cooling below T_b, c_{12} is feebly softened up to T^*, below which it hardens up to T_m. On the other hand, c_{13} exhibits great softening on cooling below T_b, which is reduced significantly at T^* and followed by pronounced hardening when approaching T_m. This suggests the increased suppression of phase diagonal orientations of PNRs near T_m.[62]

It is interesting to note that above T_b, the temperature evolution of elastic constants c_{13} and c_{33} is not following normal behavior but showing hardening until a temperature of ∼1200 K. This slight hardening above T_b is quite unexpected, because above T_b the region is simply the paraelectric phase. Such behavior has also been reported for TTB SBN and was correlated with the possible existence of an additional relaxation process other than that of PNRs above T_b.[63]

Anisotropy of longitudinal elastic stiffness is a useful aid to visualize material's anisotropy, which is provided by the system of principal bond chains (PBCs) described by the PBC vectors.[64] Fig. 5 shows the anisotropy of longitudinal elastic stiffness of CBN at selected temperatures, revealing a continuous change below T_b on cooling along and perpendicular to the c-axis. A clear signature relating to the initiation of freezing of PNRs at ∼800 K can be seen in the plane perpendicular to the c-axis, where a major suppression of anisotropy is observed. The values of $c'_{\max}/c'_{\min}$ (where $c'_{\max}$ and $c'_{\min}$ are the maximum and minimum values, respectively, of longitudinal elastic stiffness coefficients in a plane) from these diagrams (Fig. 5) give a clear hint about the elastic anisotropy. Selected values for $c'_{\max}/c'_{\min}$ are given in Table II, stating that the anomaly is big near T^* (∼800 K) and further increases when

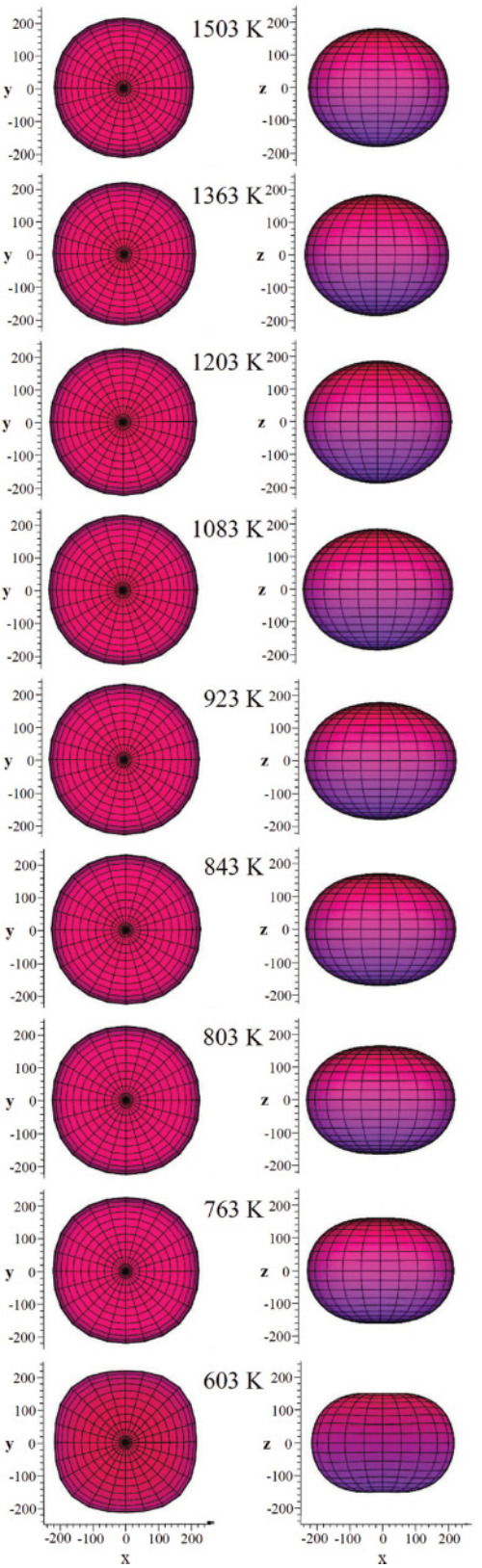

FIG. 5. (Color online) Projection of the representation surface of the longitudinal elastic stiffness of CBN along [001] and [010] at selected temperatures. The labeling x, y, and z of the axes correspond to axes $e1$, $e2$, and $e3$ of the Cartesian reference system. Units are in gigapascals. The anisotropy changes its shape significantly ∼800 K, showing suppressions along and perpendicular to the c-axis.

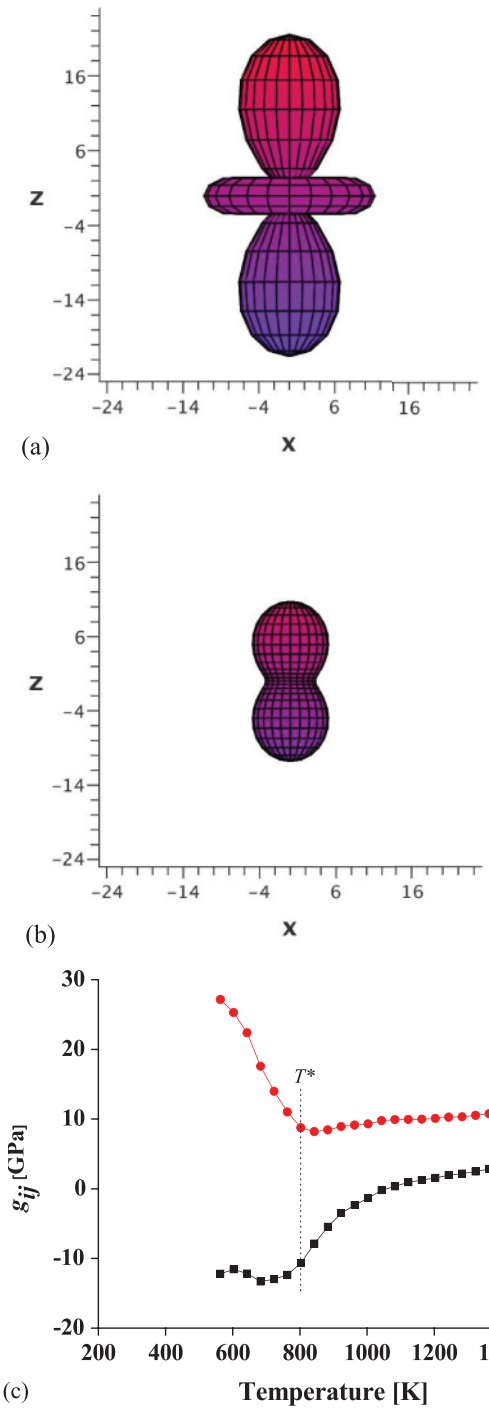

FIG. 6. (Color online) Longitudinal effect of the deviation from Cauchy relations at (a) $T = 603$ K and (b) $T = 1503$ K, and (c) temperature dependence of the deviation from Cauchy relations for CBN.

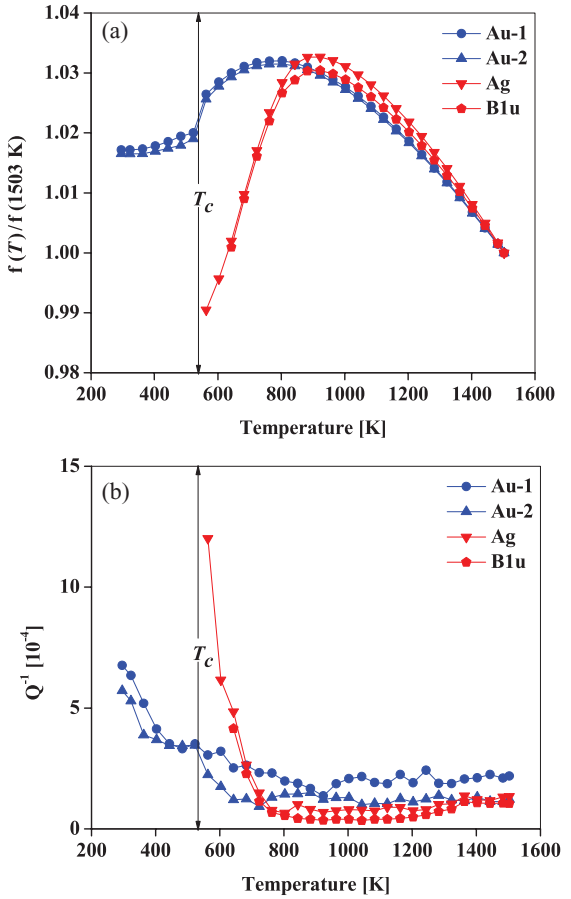

FIG. 7. (Color online) (a) Temperature evolution of selected resonance modes, and (b) corresponding inverse quality factor for CBN.

approaching phase transition. This behavior below ~800 K is in accordance to the evolution of thermal expansion and elastic constants measurements.

Hints at the nature of the bonding interactions in crystals can be obtained by the deviation from Cauchy relations[65] represented by the second-rank tensor invariant g_{ij}. It is already known that the Cauchy relations are fulfilled only under certain conditions (only central forces, all lattice particles are located on inversion centers, no anharmonicity, no thermal vibrations, etc.); i.e., all g_{ij} vanish.[65,66] The experimental data show that the Cauchy relations are more or less strongly violated in all crystal species. The deviation from Cauchy relations for CBN crystals is shown in Fig. 6. It can be seen that at high temperatures the anisotropy is quite small and both independent g_{ij} values are positive. Although g_{ij} values are related to the bonding interactions, here they are also giving a clear signature of T^* in the temperature evolution of g_{ij} where it deviates from its normal path at ~800 K. The positive value of g_{33} near T_c states that the directional bonding contribution within the (001) plane is reduced and that simultaneously nondirectional bonding contribution is increased. However, the negative value of g_{11} ($=g_{22}$) states that parallel to the fourfold axis, the directional bonding contributions are dominant when approaching T_c. It is well known that long-range coulomb forces favor stability of the ferroelectric state.[67] A closer examination of Fig. 6 reveals this phenomenon near T_c, where the positive value of g_{33} indicates the development of strong nondirectional bonding (coulomb interaction) within the (001) plane, resulting in the ferroelectric phase in CBN.

The temperature dependence of selected resonance modes (taken from Fig. 1) of CBN and their inverse quality factors (Q^{-1}) related to the sharpness of the resonances are shown in Fig. 7. The observed modes of CBN can roughly be divided

in two groups characterized by two behaviors near ∼800 K. Modes of the first group (Ag and B_1u modes) display strong softening, while modes belonging to second group (Au-1 and Au-2) show only moderate softening below ∼800 K. Most modes of group 2 are still observable in the ferroelectric phase, as they are dominated by the shear stiffness coefficients c_{44} and c_{66}, which are nearly unaffected by the mechanical interactions during the phase transitions. In the ferroelectric phase, the dissipation effects are so strong that modes of group 1 are no longer observable; these modes are probably more influenced by longitudinal elastic stiffness and transverse interaction coefficients.

The resonance behavior in the low-temperature ferroelectric phase is characterized by strong and highly anisotropic ultrasound attenuation, which is probably caused by growing influence of the quasistatic-to-static PNRs below T_m, or anelastic interactions between elastic waves and ferroelectric domain walls (i.e., there is an energy loss of ultrasound waves due to back-and-forth domain wall movement by the elastic waves), or may be both. Therefore, in the vicinity of the ferroelectric phase transition and in the ferroelectric phase, only 10–12 resonance peaks (see the resonance spectra of CBN below the red line in Fig. 1) was observed. Thus, CBN crystals in their raw (as-grown) form are not suitable to measure their elastic properties in their ferroelectric phase. Poling the CBN single crystal is a potential approach to overcome this problem.

IV. CONCLUSIONS

The relaxor phenomena for as-grown CBN single crystals was explored from thermal expansion measurements, which revealed the existence of characteristic temperatures T_b, T^*, and T_m. Temperatures for T_b, T^*, and T_m were observed ∼1100 K, ∼800 K, and ∼600 K, respectively. Moreover, occurrence of a diffuse relaxor-to-ferroelectric phase transition in unpoled CBN was suggested.

Highly precise temperature dependence of the full set of elastic constants c_{ij} for CBN single crystals was measured, and the influence of PNRs on the elastic properties was studied in detail. Large elastic anisotropy was observed for all elastic constants. Furthermore, the anisotropy of longitudinal elastic stiffness and the deviation from Cauchy relations showed a clear signature of T^* where first freezing of PNRs begins. The presence of T^* in TTB CBN indicated that this temperature is not just a particular feature of the lead-based relaxors but represents a fundamental property of a broad range of relaxor compounds.

*chandrashekhar.pandey@ruhr-uni-bochum.de
†schreuer@rub.de

[1] G. A. Samara, J. Phys. Condens. Matter **15**, R367 (2003), and references therein.
[2] L. E. Cross, Ferroelectrics **76**, 241 (1987).
[3] A. S. Bhalla, R. Guo, and R. Roy, Mater. Res. Innovat. **4**, 3 (2000).
[4] J. F. Scott, J. Phys. Condens. Matter **18**, R361 (2006).
[5] G. Burns and F. H. Dacol, Phys. Rev. B **28**, 2527 (1983); Solid State Comm. **48**, 853 (1983).
[6] W. Westphal and W. Kleemann, Phys. Rev. Lett. **68**, 847 (1992).
[7] I.-K. Jeong, T. W. Darling, J. K. Lee, Th. Proffen, and R. H. Heffner, Phys. Rev. Lett. **94**, 147602 (2005), and reference therein.
[8] A. A. Bokov and Z.-G. Ye, J. Mater. Sci. **41**, 31 (2006), and reference therein.
[9] D. La-Orauttapong, J. Toulouse, J. L. Robertson, and Z.-G. Ye, Phys. Rev. B **64**, 212101 (2001).
[10] D. La-Orauttapong, J. Toulouse, Z.-G. Ye, W. Chen, R. Erwin, and J. L. Robertson, Phys. Rev. B **67**, 134110 (2003).
[11] O. Svitelskiy, J. Toulouse, G. Yong, and Z.-G. Ye, Phys. Rev. B **68**, 104107 (2003).
[12] J. Toulouse, F. Jiang, O. Svitelskiy, W. Chen, and Z.-G. Ye, Phys. Rev. B **72**, 184106 (2005).
[13] O. Svitelskiy, D. La-Orauttapong, J. Toulouse, W. Chen, and Z.-G. Ye, Phys. Rev. B **72**, 172106 (2005).
[14] E. Dul'kin, M. Roth, P.-E. Janolin, and B. Dkhil, Phys. Rev. B **73**, 012102 (2006).
[15] M. Roth, E. Mojaev, E. Dul'kin, P. Gemeiner, and B. Dkhil, Phys. Rev. Lett. **98**, 265701 (2007).
[16] B. Mihailova, B. Maier, C. Paulmann, T. Malcherek, J. Ihringer, M. Gospodinov, R. Stosch, B. Güttler, and U. Bismayer, Phys. Rev. B **77**, 174106 (2008).
[17] B. Dkhil, P. Gemeiner, A. Al-Barakaty, L. Bellaiche, E. Dul'kin, E. Mojaev, and M. Roth, Phys. Rev. B **80**, 064103 (2009).
[18] S. Tsukada, Y. Terado, C. Moriyoshi, Y. Kuroiwa, and S. Kojima, IEEE Trans. Ultrason. Ferroelectrics Freq. Contr. **57**, 2159 (2010).
[19] S. D. Prokhorova and S. G. Lushnikov, Ferroelectrics **90**, 187 (1989).
[20] H. Arndt and F. Schmidt, Ferroelectrics **79**, 149 (1988).
[21] A. S. Bhalla, R. Guo, L. E. Cross, G. Burns, F. H. Dacol, and R. R. Neurgaonkar, Phys. Rev. B **36**, 2030 (1987).
[22] J. J. De. Yoreo, R. O. Pohl, and G. Burns, Phys. Rev. B **32**, 5780 (1985).
[23] Y. Moriya, H. Kawaji, T. Tojo, and T. Atake, Phys. Rev. Lett. **90**, 205901 (2003).
[24] D. Viehland, J. F. Li, S. J. Jang, L. E. Cross, and M. Wuttig, Phys. Rev. B **46**, 8013 (1992).
[25] D. Viehland, S. J. Jang, M. Wuttig, and L. E. Cross, J. Appl. Phys. **68**, 2916 (1990).
[26] V. A. Bokov and I. E. Myl'nikova, Fiz. Tverd. Tela (Leningrad) **3**, 841 (1961) [Sov. Phys. Solid State **3**, 613 (1961)].
[27] J. Kuwata, K. Uchino, and S. Nomura, Ferroelectrics **22**, 863 (1979).
[28] Y. Xi, C. Zhili, and L. E. Cross, J. Appl. Phys. **54**, 3399 (1983).
[29] S. Kamba, V. Bovtun, J. Petzelt, I. Rychetsky, R. Mizaras, A. Brilingas, J. Banys, J. Grigas, and M. Kosec, J. Phys. Condens. Matter **12**, 497 (2000).
[30] A. M. Glass, J. Appl. Phys. **40**, 4699 (1969).
[31] R. R. Neurgaonkar, W. F. Hall, J. R. Oliver, W. W. Ho, and W. K. Cory, Ferroelectrics **87**, 167 (1988).
[32] K. Tada, T. Murai, A. Aoki, K. Muto, and K. Awazu, Jpn. J. Appl. Phys. **11**, 1622 (1972).
[33] R. R. Neurgaonkar, W. K. Cory, and J. R. Oliver, Ferroelectrics **51**, 3 (1983).

[34]B. Fischer, M. Cronin-Golomb, J. O. White, A. Yariv, and R. R. Neurgaonkar, Appl. Phys. Lett. **40**, 863 (1982).
[35]R. R. Neurgaonkar, W. K. Cory, J. R. Oliver, M. D. Ewbank, and W. F. Hall, Opt. Eng. **26**, 392 (1987).
[36]F. Kahmann, J. Höhne, R. Pankrath, and R. A. Rupp, Phys. Rev. B **50**, 2474 (1994).
[37]M. Wesner, C. Herden, R. Pankrath, D. Kip, and P. Moretti, Phys. Rev. E **64**, 036613 (2001).
[38]R. R. Neurgaonkar, M. H. Kalisher, T. C. Lim, E. J. Staples, and K. L. Keester, Mater. Res. Bull. **15**, 1235 (1980).
[39]W. P. Mason, *Piezoelectric Crystals and their Applications to Ultrasonics* (Van Nostrand, New York, 1950).
[40]M. Burianek, B. Joschko, I. Kerkamm, T. Schoenbeck, D. Klimm, and M. Muehlberg, J. Cryst. Growth **299**, 413 (2007).
[41]I. G. Ismailzade, Kristallografiya **5**, 268 (1960).
[42]M. Eßer, M. Burianek, D. Klimm, and M. Mühlberg, J. Cryst. Growth **240**, 1 (2002).
[43]Y. J. Qi, C. J. Lu, J. Zhu, X. B. Chen, H. L. Song, H. J. Zhang, and X. G. Xu, Appl. Phys. Lett. **87**, 082904 (2005).
[44]Y. Xu, *Ferroelectric Materials and Their Applications* (North-Holland, Amsterdam 1991).
[45]A. Glass, Appl. Phys. Lett. **13**, 147 (1968).
[46]H. Song, H. Zhang, X. Xu, X. Hu, X. Cheng, J. Wang, and M. Jiang, Mater. Res. Bull. **40**, 643 (2005).
[47]M. Mühlberg, M. Burianek, B. Joschko, D. Klimm, A. Danilewsky, M. Gelissen, V. L. Bayarjargal, G. Görler, and B. Hildmann, J. Cryst. Growth **310**, 2288 (2008).
[48]A. Migliori and J. Sarrao, *Resonant Ultrasound Spectroscopy* (John Wiley & Sons, New York, 1997); A. Migliori, J. L. Sarrao, W. M. Visscher, T. M. Bell, M. Lei, Z. Fisk, and R. G. Leisure, Phys. B Condens. Matter **183**, 1 (1993).
[49]J. Schreuer, IEEE Trans. Ultrason. Ferroelectrics Freq. Contr. **49**, 1474 (2002).
[50][http://www.netzsch.de].
[51][http://www.nfcorp.co.jp/english].
[52]N. M. Shorrocks, R. W. Whatmore, and F. W. Ainger, Ultrason. Symp. Proc. 359 (1982).
[53]S. Haussühl, *Physical Properties of Crystals* (Wiley-VCH, Weinheim, 2007).
[54]J. Schreuer and S. Haussühl, Eur. Mineral. Union Notes Mineral. **7**, 173 (2005).
[55]J. L. Cao, L. T. Li, Y. L. Wang, J. Q. Zhao, and Z. L. Gui, J. Mater. Sci. **37**, 3225 (2002).
[56]P. Reiche, R. Schalge, J. Bohm, and D. Schultze, Kristall und Technik **15**, 23 (1980).
[57]R. R. Neurgaonkar, L. E. Cross, W. F. Hall, and W. W. Ho, Technical Report, (Rockwell International Science Center, Thousand Oaks, California, 1983), pp. 13.
[58]J. F. Nye, *Physical Properties of Crystals* (Clarendon Press Oxford, New York, 1987).
[59]J. Schefer, D. Schaniel, V. Pomjakushin, U. Stuhr, V. Petricek, Th. Woike, M. Wöhlecke, and M. Imlau, Phys. Rev. B **74**, 134103 (2006).
[60]F. Prokert, J. Ihringer, and H. Ritter, Ferroelectrics Lett. **20**, 73 (1995).
[61]F. Prokert, J. Ihringer, and H. Ritter, Ferroelectrics Lett. **24**, 1 (1998).
[62]O. Svitelskiy, A. V. Suslov, J. B. Betts, A. Migliori, G. Yong, and L. A. Boatner, Phys. Rev. B **78**, 064113 (2008).
[63]J. H. Ko, D. H. Kim, and S. Kojima, Phys. Rev. B **77**, 104110 (2008).
[64]J. Schreuer and S. Haussühl, Eur. Mineral. Union Notes Mineral. **7**, 97 (2005).
[65]S. Haussühl, Phys. Kondens. Mater. **6**, 181 (1967).
[66]M. Born and K. Huang, *Dynamical Theory of Crystal Lattices* (Clarendon Press, Oxford, 1954).
[67]R. E. Cohen, Nature **358**, 136 (1992).